






Article

Experimental and Theoretical Study of Photoionization of Cl III

Sultana N. Nahar ¹, Edgar M. Hernández ², David Kilkoynne ^{3,†}, Armando Antillón ⁴, Aaron M. Covington ⁵, Olmo González-Magaña ⁴, Lorenzo Hernández ⁴, Vernon Davis ⁵, Dominic Calabrese ⁶, Alejandro Morales-Mori ⁴, Dag Hanstorp ⁷, Antonio M. Juárez ⁴ and Guillermo Hinojosa ^{4,*}

- ¹ Department of Astronomy, The Ohio State University, Columbus, OH 43210, USA
² Centro de Investigación en Ciencias-IICBA, Universidad Autónoma del Estado de Morelos, Cuernavaca 62209, Mexico
³ The Advanced Light Source, Lawrence Berkeley National Laboratory, CA 94720, USA
⁴ Instituto de Ciencias Físicas, Universidad Nacional Autónoma de México, A. P. 48-3, Cuernavaca 62251, Mexico
⁵ Physics Department, University of Nevada, Reno, NV 89557-0220, USA
⁶ Department of Physics, Sierra College, Rocklin, CA 95677, USA
⁷ Department of Physics, University of Gothenburg, SE-412 96 Gothenburg, Sweden
* Correspondence: hinojosa@icf.unam.mx
† Deceased.

Abstract: Photoionization of Cl III ions into Cl IV was studied theoretically using the ab initio relativistic Breit–Pauli R-matrix (BPRM) method and experimentally at the Advanced Light Source (ALS) synchrotron at the Lawrence Berkeley National Laboratory. A relative-ion-yield spectrum of Cl IV was measured with a photon energy resolution of 10 meV. The theoretical study was carried out using a large wave-function expansion of 45 levels of configurations $3s^23p^2$, $3s3p^3$, $3s^23p3d$, $3s^23p4s$, $3s3p^23d$, and $3p^4$. The resulting spectra are complex. We have compared the observed spectrum with photoionization cross sections (σ_{PI}) of the ground state $3s^23p^3(^4S_{3/2}^o)$ and the seven lowest excited levels $3s^23p^3(^2D_{5/2}^o)$, $3s^23p^3(^2D_{3/2}^o)$, $3s^23p^3(^2P_{3/2}^o)$, $3s^23p^3(^2P_{1/2}^o)$, $3s3p^4(^4P_{5/2})$, $3s3p^4(^4P_{3/2})$ and $3s3p^4(^4P_{1/2})$ of Cl III, as these can generate resonances within the energy range of the experiment. We were able to identify most of the resonances as belonging to various specific initial levels within the primary Cl III ion beam. Compared to the first five levels, resonant structures in the σ_{PI} of excited levels of $3s3p^4$ appear to have a weaker presence. We have also produced combined theoretical spectra of the levels by convolving the cross sections with a Gaussian profile of experimental width and summing them using statistical weight factors. The theoretical and experimental features show good agreement with the first five levels of Cl III. These features are also expected to elucidate the recent observed spectra of Cl III by Sloan Digital Scan Survey project.

Keywords: relativistic multi-configurations interaction; R-matrix method; photoionization; phosphorus isoelectronic ion Cl IV; merged-beams technique



Citation: Nahar, S.N.; Hernández, E.M.; Kilkoynne, D.; Antillón, A.; Covington, A.M.; González-Magaña, O.; Hernández, L.; Davis, V.; Calabrese, D.; Morales-Mori, A.; et al. Experimental and Theoretical Study of Photoionization of Cl III. *Atoms* **2023**, *11*, 28. <https://doi.org/10.3390/atoms11020028>

Academic Editor: Eugene T. Kennedy

Received: 8 December 2022

Revised: 3 January 2023

Accepted: 8 January 2023

Published: 3 February 2023



Copyright: © 2023 by the authors. Licensee MDPI, Basel, Switzerland. This article is an open access article distributed under the terms and conditions of the Creative Commons Attribution (CC BY) license (<https://creativecommons.org/licenses/by/4.0/>).

1. Introduction

The Io satellite plasma torus in Jupiter is a ring-shaped cloud of plasma in which Cl III ions were discovered by the Far Ultraviolet Spectroscopic Explorer (FUSE) [1,2] and also by the Galileo probe [3]. In addition, the CORONAS-F spacecraft has detected high-charge states of chlorine in coronal solar flares [4]. The apparently large abundance of chlorine in the interstellar medium is an unresolved question in astrophysics [5] prompting the need for more investigations into the fundamental properties of this element. In general, measurements of photoionization spectra of ions of chlorine [6] have helped in benchmarking theoretical efforts such as those of the OPACITY [7–9], IRON [10], and NORAD [11] projects that have for several decades focused on understanding the interaction of photons with ions.

Photoionization and spectroscopic data on chlorine ions remain rare. Experimental efforts have provided lifetimes and oscillator strengths for specific transitions observed by FUSE [12] for Cl II ions. A multi-configuration Hartree–Fock approach [13] showed a strong correlation between Rydberg series and perturbed states for the case of singly-ionized chlorine. An experimental effort investigating the photoionization of Cl II from threshold to 28 eV offered Rydberg series resonance energies and cross sections [6]. This investigation was followed by large-scale Dirac Coulomb R-matrix calculations [7,14], rendering an identification for the observed spectrum.

In the present study, we present a measurement of the relative ion yield resulting from the single-photon photoionization of Cl III. The data consists of the effective current of the Cl IV ions as a function of the photon beam energy. Photoionization can proceed via a direct process as in the following,



where $h\nu$ represents the photon (giving the background cross section), or through an intermediate autoionizing state at an energy belonging to a Rydberg series state,



which introduces a resonance in the cross section. The introduction of an intermediate state for resonances can be studied naturally by the close-coupling (CC) approximation and the R-matrix method. This report presents resonant features in the measured photoionization cross section of Cl III, studied theoretically using the relativistic Breit–Pauli R-matrix (BPRM) method; the experimental and theoretical results are each benchmarked against the other. Cl III is isoelectronic to phosphorous. For this reason, the photoionization study of atomic phosphorus by Berkowitz and collaborators [15] is relevant to the present work. We point out that the spectroscopy of elements isoelectronic to phosphorus is also relevant in astrobiology. Because phosphorus is one of the basic elements of life, its spectroscopic features are used to label phosphorus-containing exoplanetary atmospheres as possible life sustaining regions (e.g., Ref. [16]).

2. Theoretical Study with Breit–Pauli R-Matrix Method

The theoretical study was carried out using the relativistic Breit–Pauli R-matrix (BPRM) method with a large close-coupling (CC) wavefunction expansion that includes 45 levels of the core ion Cl IV. It is the core ion excitation that enables autoionizing resonances in photoionization cross sections. A brief outline of the method is given below.

In the CC approximation, the atomic system has (N+1) electrons and the core (or ‘target’) ion is an N-electron system interacting with the (N+1)th electron. The (N+1)th electron is bound or in the continuum depending on whether its energy E is negative or positive, respectively. The total wave function Ψ_E , of $SL\pi J$ symmetry, is expressed by an expansion of the form (e.g., Ref. [17])

$$\Psi_E(e^- + ion) = A \sum_i \chi_i(ion)\theta_i + \sum_j c_j \Phi_j, \tag{3}$$

where the core ion eigenfunction χ_i represents the ground and various excited states. The sum is over the number of states considered. The core is coupled with the (N+1)th electron function θ_i . The (N+1)th electron (of kinetic energy k_i^2) is in a channel labeled as $S_i L_i \pi_i J_i k_i^2 \ell_i (SL\pi J)$. A is the anti-symmetrization operator. In the second sum, the Φ_j are bound-channel functions of the (N+1)-electron system that provides the orthogonality between the continuum and the bound electron orbitals, and accounts for short-range correlations.

Substitution of $\Psi_E(e^- + ion)$ in the Schrödinger equation

$$H_{N+1}\Psi_E = E\Psi_E, \tag{4}$$

introduces a set of coupled equations that are solved using the R-matrix approach. This approach divides the space into an inner space of radius r_a that includes all short-range interactions, and an outer space up to infinity where the wavefunction is treated as Coulombic (e.g., Refs. [8,17–20]). The relativistic effects are included through Breit–Pauli approximation (e.g., Ref. [17]), in which the Hamiltonian is given by

$$H_{N+1}^{BP} = \sum_{i=1}^{N+1} \left\{ -\nabla_i^2 - \frac{2Z}{r_i} + \sum_{j>i}^{N+1} \frac{2}{r_{ij}} \right\} + H_{N+1}^{mass} + H_{N+1}^{Dar} + H_{N+1}^{so}, \quad (5)$$

in Rydberg units. The relativistic correction terms are corrected by a mass term, $H^{mass} = -\frac{\alpha^2}{4} \sum_i p_i^4$, the Darwin term, $H^{Dar} = \frac{Z\alpha^2}{4} \sum_i \nabla^2(\frac{1}{r_i})$, and a spin-orbit interaction term, $H^{so} = Z\alpha^2 \sum_i \frac{1}{r_i^3} \mathbf{l}_i \cdot \mathbf{s}_i$. The R-matrix Breit–Pauli (BPRM) approximation also includes parts of several two-body interaction terms, such as those without the momentum operators [17].

The solution of the BRPM approximation is a continuum wave function Ψ_F for an electron with positive energies ($E > 0$), or a bound state Ψ_B at a negative total energy ($E \leq 0$). The complex resonant structures in the photoionization spectra are produced from channel couplings between continuum channels that are open ($k_i^2 > 0$), and ones that are closed ($k_i^2 < 0$), at electron energies k_i^2 corresponding to autoionizing states of the Rydberg series $S_i L_i J_i \pi_i \nu \ell$. ν is the effective quantum number of the series converging to excited core thresholds.

The photoionization cross section (σ_{PI}) is given by (e.g., Ref. [17])

$$\sigma_{PI} = \frac{4\pi^2}{3c} \frac{1}{g_i} \omega \mathbf{S}, \quad (6)$$

where g_i is the statistical weight of the bound state, ω is the incident photon energy, and \mathbf{S} is the generalized line strength

$$\mathbf{S} = | \langle \Psi_j || \mathbf{D}_L || \Psi_i \rangle |^2 = \left| \left\langle \psi_f \left| \sum_{j=1}^{N+1} r_j \right| \psi_i \right\rangle \right|^2. \quad (7)$$

Here Ψ_i and Ψ_f are the initial and final state wave functions, respectively, and \mathbf{D}_L is the dipole operator in the length form.

3. Computation of Photoionization Cross Sections

BPRM computations were carried out through the package of R-matrix codes [20–22], which consists of several stages. The computation starts with the wave-function expansion of the core ion as the initial input. For this wave function, an atomic structure calculation was carried out using the code SUPERSTRUCTURE (SS) [23,24]. SS uses a Thomas–Fermi–Dirac–Amaldi potential and includes relativistic contributions in a Breit–Pauli approximation in which a full Breit interaction and parts of two-body correction terms are included. A set of 13 configurations of the core ion Cl IV was optimized to obtain the wave-function expansion for Cl III. The configurations, which include orbitals up to the 4d, are $3s^2 3p^2$, $3s 3p^3$, $3s^2 3p 3d$, $3s^2 3p 4s$, $3s^2 3p 4p$, $3s^2 3p 4d$, $3s 3p^2 3d$, $3s 3p^2 4s$, $3s 3p^2 4p$, $3p^4$, $3p^3 3d$, $3p^3 4s$, and $3p^3 4p$. Table 1 presents 45 (the ground and 44 excited) fine-structure levels of Cl IV included in the wave-function expansion of Cl III. The calculated energies from SS are compared with observed values [25] (listed in the NIST [26] compilation). A comparison shows the agreement between SS and the observed values to within a few percent to a larger number, and some, e.g., $3p^4(^3P_{0,1,2})$, are over 10%. SS is not adjusted for any observed values. The optimization for energies and wavefunctions is carried out through the number of configurations and by varying the orbital wavefunctions with Thomas–Fermi scaling parameters. SS computes the radial wavefunction of all orbitals which remain the same while the energies change with the angular momenta of the states. The present set of energies is the resultant of efforts to reach an overall agreement between the calculated and

measured values instead of focusing to improve any small set of energies, and the optimized set of configurations is selected for manageable computation by the R-matrix codes, which will retain all important physical characteristics of the atomic process. The accuracy of results provided by the R-matrix method is much improved over those of core ion energies since the method can handle a much larger set of configurations, e.g., 47 configurations of the core ion and interacting electron were used to compute the photoionization cross sections of Cl III. Hence, the effect of uncertainties in the core ion wavefunctions were reduced considerably by the R-matrix computations and resulted in a good agreement between the calculated and experimental σ_{PI} .

Table 1. The 45 levels of Cl IV that were included in the CC wavefunction expansion for Cl III. The calculated energies in Ry obtained from SUPERSTRUCTURE (SS) are compared with the measured values [25] available in the NIST [26] compilation table.

	Config	SL π	2J	E (NIST, Ry)	E (SS, Ry)
1	3s ² 3p ²	³ P	0	0.0	0.0
2	3s ² 3p ²	³ P	2	0.004483	0.004553
3	3s ² 3p ²	³ P	4	0.012228	0.012601
4	3s ² 3p ²	¹ D	4	0.125460	0.153621
5	3s ² 3p ²	¹ S	0	0.296597	0.350797
6	3s3p ³	⁵ S ^o	4	0.592325	0.587425
7	3s3p ³	³ D ^o	2	0.93635	1.116700
8	3s3p ³	³ D ^o	4	0.93666	0.911418
9	3s3p ³	³ D ^o	6	0.93741	0.912132
10	3s3p ³	³ P ^o	4	1.09585	1.090706
11	3s3p ³	³ P ^o	2	1.09602	1.091088
12	3s3p ³	³ P ^o	0	1.09625	1.091201
13	3s ² 3p3d	¹ D ^o	4	1.09625	1.201007
14	3s3p ³	³ S ^o	2	1.482837	1.509883
15	3s ² 3p3d	³ F ^o	4		1.482837
16	3s ² 3p3d	³ F ^o	6		1.487126
17	3s ² 3p3d	³ F ^o	8		1.492982
18	3s3p ³	¹ P ^o	2	1.51946	1.589771
19	3s ² 3p3d	³ P ^o	4	1.65525	1.775908
20	3s ² 3p3d	³ P ^o	2	1.65917	1.779791
21	3s ² 3p3d	³ P ^o	0	1.66124	1.781748
22	3s ² 3p3d	³ D ^o	2	1.70414	1.814810
23	3s ² 3p3d	³ D ^o	4	1.70565	1.816602
24	3s ² 3p3d	³ D ^o	6	1.70722	1.817951
25	3s3p ³	¹ D ^o	4		1.806554
26	3s ² 3p3d	¹ F ^o	6		1.980420
27	3s ² 3p4s	³ P ^o	0	1.959461	1.987296
28	3s ² 3p4s	³ P ^o	2	1.962772	1.991670
29	3s ² 3p4s	³ P ^o	4	1.972602	1.999506
30	3s ² 3p4s	¹ P ^o	2	1.99981	1.970271
31	3s ² 3p3d	¹ P ^o	2		2.087061
32	3s3p ² 3d	⁵ F	2		2.115199
33	3s3p ² 3d	⁵ F	4		2.116611
34	3s3p ² 3d	⁵ F	6		2.118763
35	3s3p ² 3d	⁵ F	8		2.121696
36	3s3p ² 3d	⁵ F	10		2.125465
37	3p ⁴	¹ D	4		2.147704
38	3s3p ² 3d	⁵ D	0		2.174180
39	3s3p ² 3d	⁵ D	2		2.174565
40	3s3p ² 3d	⁵ D	4		2.175339
41	3s3p ² 3d	⁵ D	6		2.176516
42	3s3p ² 3d	⁵ D	8		2.178121
43	3p ⁴	³ P	0	2.291576	2.042081
44	3p ⁴	³ P	2	2.293894	2.039031
45	3p ⁴	³ P	4	2.300008	2.032375

Photoionization cross sections were obtained with the inclusion of the radiation damping effects [22]. For precise positions of the resonances, the calculated core ion excitation energies were replaced by the available observed energies and the cross sections were

shifted to match the measured ionization energies of the levels. These cross sections were compared directly with the measured cross sections for identification of the resonances of various levels to which they may belong. The cross sections were also convolved with a Gaussian profile of width of 10 meV using the program GUSAVPX [27] for comparison with the observed spectral features in the experiment. However, the width was varied in a few instances to avoid significant dissolution of resonances.

4. Experiment

A photon beam and a Cl III ion beam propagating in opposite directions were merged over a common collinear path. As a consequence of their interaction, ions from the Cl III ion beam are photoionized, yielding Cl IV. The resulting ions were separated from the parent ion beam and counted. Relevant parameters of both beams and their overlap were monitored.

The experiment was implemented in the now decommissioned ion-photon beam end-station at the Advanced Light Source (ALS) at Lawrence Berkeley National Laboratory. This technique was based on the merged-beams technique [28] and was described in more detail in previous measurements of the photoionization of Ne⁺ [29] and Se⁺ [30]. A short description of the experimental technique with some details pertinent to the present study is presented.

The Cl III ion beam was generated with an ECR ion source. This ion source had an insertion oven in which a small sample of FeCl₃ was evaporated and ionized in the chamber by collisions with the ECR electrons. Ions were then extracted from the ion source by a repulsive potential of 6 kV. These ions were mass-to-charge selected by a 90° bending electromagnet. The mass resolution of the electromagnet is sufficient to discern and therefore discard any possible contamination of the Cl III ($m/q = 17.73$) ion beam with O⁺ ($m/q = 16$).

Next, a set of electrostatic lenses focused the ion beam into the center of a voltage-biased cylindrical mesh located in a chamber of the experiment where the ions were merged with photons from the ALS (for the ions to reach this chamber, they were first deflected by a set of 90° spherical electrostatic bending plates). In this chamber, Cl III ions were ionized by the counter-propagating photons. In the following stage, a second electromagnet served to separate the Cl IV ions from the parent Cl III ions. Cl IV ions were counted using electrons emitted from an emission-biased metal plate located in front of a channel electron multiplier plate. A typical Cl III ion beam current was 50 nA.

The photon beam was generated by a 10-cm-period undulator installed in the trajectory of a constant current of 0.5 A in the 1.9 GeV synchrotron storage ring, producing a collimated photon beam of width less than 1 mm and with a divergence less than 0.05°. This photon beam was then incident onto a grazing spherical-grating monochromator. The photon energy was scanned by rotating the grating and translating the exit slit of the monochromator while adjusting the undulator gap to maximize the photon beam intensity.

The photon flux was measured with a calibrated silicon photodiode [30] with a 5% uncertainty. A precision current meter provided a normalization signal to the data acquisition system. The photon beam was mechanically pulsed using a controlled chopper-wheel to separate the Cl IV signal ions produced by photoionization from those produced by collisions with the residual gas in the apparatus.

In this experiment, absolute cross sections were not measured. The reported measured intensity is therefore arbitrary. However, the signal was normalized to the ion beam current and to the photon beam current. The photon beam current was corrected by the number of photons or via the known quantum efficiency of the photon silicon diode detector as a function of the photon energy. Due to the presence of higher-order components in the photon beam [31], the error in the intensity can be large. However, this experiment is concerned primarily with the energy resonances, so the corrections to the photon beam intensity will not be discussed here.

The photon energy was nominally established by the rotating-grating control system. Further calibration with an ionization gas-cell increased the accuracy of the measured photon energy. This calibration was accomplished by using the ionization energies for He [32] and Kr [33] as references in the energy interval from 21.218 eV to 63.355 eV. We estimate that the photon energy error, from this technique, has a maximum value of ± 10 meV. This same energy calibration technique was employed for the single-photon photoionization spectrum measurement of Cl^+ [6], achieving an agreement with the NIST data base [26] out to three decimal places (in eV).

5. Results

We present the photoionization spectrum of Cl III with resonant features (as defined in the introduction) studied both experimentally and theoretically, and benchmarked with each other. The measured spectrum is the combined spectra of the ground and low-lying excited levels of Cl III that can be present in the primary beam. The theoretical spectra are obtained for each individual low-lying level and are compared with the measured one for identification of features. The results are illustrated and discussed below.

The observed spectrum, shown in Figure 1, was measured in energy-intervals of 1 eV. Each individual spectrum was overlapped with its neighbors by 0.5 eV. All the individual scans were then merged into a single spectrum after normalization. This method was employed in the early stage of the experiment and was implemented to reduce the effects of possible mechanical backlash from the monochromator positioning mechanism. The process of integrating the pieces of the spectrum was conducted by grouping the individual bins of spectra when variations among them were very small, so that their normalization factors were close to one. Whenever needed, this process of "gluing" also included small energy shifts to overlap observed resonances rather than merely combining the spectra. The overall photon energy error caused by this procedure was estimated to be no greater than ± 8 meV. Therefore, considering a ± 10 meV additional uncertainty from the gas-cell energy calibration, the total photon energy uncertainty for this experiment is ± 13 meV. The resulting measured ion-yield spectrum in Figure 1 shows several resonant series structures and a slow monotonic rise in the background.

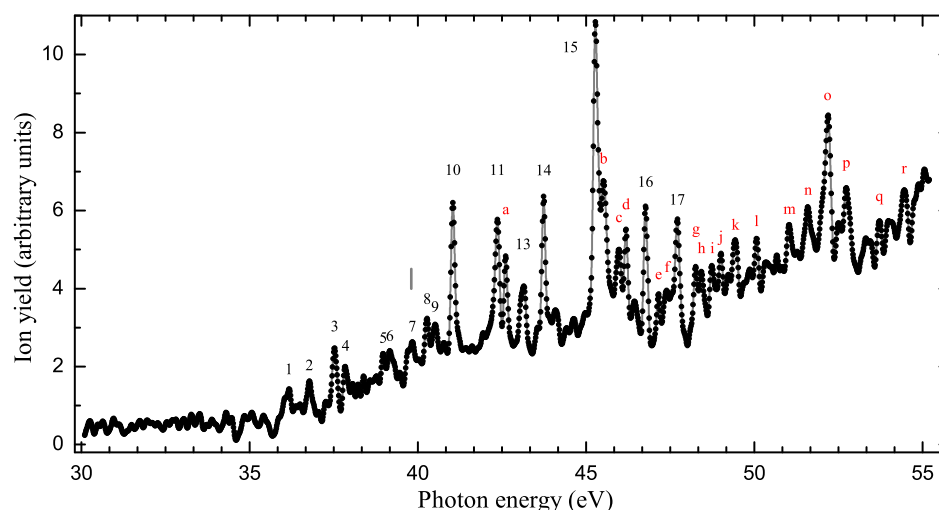


Figure 1. (Color online) Single-photon photoionization ion-yield spectrum of Cl III into Cl IV measured with a photon energy resolution of 10 meV. Measured data are (black) dots joined by a straight line. The vertical line (gray) corresponds to the ionization limit of 39.80 eV. Alpha (red) and numeric labels correspond to some of the most well-defined and prominent peaks listed in Tables 2 and 3. Labeling was arbitrarily chosen to improve clarity.

Figure 2 presents the theoretically-calculated σ_{PI} of the eight lowest levels of Cl III in various panels, ground (b) $3s^23p^3(^4S_{3/2}^o)$ and excited (c) $3s^23p^3(^2D_{5/2}^o)$, (d) $3s^23p^3(^2D_{3/2}^o)$,

(e) $3s^23p^3(^2P_{3/2}^o)$, (f) $3s^23p^3(^2P_{1/2}^o)$, (g) $3s3p^4(^4P_{5/2})$, (h) $3s3p^4(^4P_{3/2})$, (i) $3s3p^4(^4P_{1/2})$ while (panel a) presents the measured spectrum. The eight levels were selected because they can generate resonances within the energy range of the experiment. Each panel shows complex resonances formed from the Rydberg series of autoionizing levels belonging to the core ion excitations. The complexity arises from overlapping of the series of resonances. However, in each panel, one can identify the origin of resonances and features of the levels that are seen in the observed spectrum. The arrows in the panels point to identifiable resonances in the observed spectrum, as listed in Tables 2 and 3. It can be seen that there are resonances in the observed spectrum that appear in σ_{PI} of multiple levels. The low energy resonances of the 3 levels of $3s3p^4(^4P)$, $j = 1/2, 3/2, 5/2$, are much stronger in the predicated σ_{PI} compared to the peaks in the observed σ_{PI} . This can be explained by the low abundances of these excited levels in the experimental beam in the low energy region.

Table 2. Cl^{2+} single-photon photoionization resonance energies E_0 and widths derived from Gaussian fits to the resonant peaks. Labels correspond to those in Figure 1.

E_0 (eV)	Width (eV)	Label
42.605	0.103	a
45.514	0.182	b
45.963	0.135	c
46.180	0.096	d
47.147	0.102	e
47.391	0.104	f
48.255	0.072	g
48.422	0.096	h
48.740	0.139	i
49.000	0.098	j
49.425	0.256	k
50.060	0.105	l
51.034	0.148	m
51.586	0.101	n
52.177	0.126	o
52.736	0.122	p
53.715	0.237	q
54.450	0.234	r

Table 3. Cl^{2+} single-photon photoionization resonance energies E_0 and widths derived from Gaussian fits to the resonant peaks. Labels correspond to those in Figure 1.

E_0 (eV)	Width (eV)	Label
36.161	0.069	1
36.771	0.112	2
37.521	0.128	3
37.846	0.109	4
38.966	0.129	5
39.165	0.106	6
39.829	0.072	7
40.269	0.128	8
40.506	0.148	9
41.038	0.101	10
42.354	0.118	11
43.119	0.236	13
43.735	0.093	14
45.280	0.113	15
46.764	0.115	16
47.706	0.110	17

To reproduce the observed features, the calculated single-photon photoionization cross sections of each level were convolved with a Gaussian profile of (experimental beam) width of 10 meV. No percentage contributions were considered since the abundances are not known. For each LS state, the convolved σ_{PI} of its component fine structure levels were

added with statistical weight factors and then all the cross sections were summed together. The resultant spectra are presented in Figure 3. While (panel a) presents the measured cross sections, (panel b) presents the summed features from the convolved σ_{PI} of the five lowest initial levels of states $^4S^\circ$, $^2D^\circ$, and $^2P^\circ$, and (panel c) corresponds to the summed σ_{PI} of the three 4P initial levels. The same set of arrows pointing identifiable resonances are also displayed here. The overall agreement for the existences of the resonances between the predicted and observed spectra, except for the heights of the resonances, is illustrated much better in this figure. Almost all observed resonances are accounted for in the predicted cross sections.

The measured cross sections show a monotonic rising background in Figure 1, which appeared to be an artifact of the measurement technique or of the normalization procedure. This trend can be explained to be real. We used the same normalization procedure which is identical to that used for several other measurements in which this tendency was not observed. Of particular relevance is the case of the photoionization of Cl II [6,7] for which the data were measured under the same experimental conditions as of Cl III. The rising trend was not observed in that experiment. The origin in the present spectrum is not obvious from the calculated cross sections of individual levels in Figure 2. However, the background of the summed cross sections convolved with the measured width in Figure 3 predicts such a trend, thus confirming the validity of this feature.

The present experimental photoionization spectra is comprised of the superposition of a non-resonant background signal and resonant structures. Resonant peaks are normally assigned to a Rydberg series. A Rydberg series consists of a progression of resonances at energies $E_\nu = E_c - z^2/\nu^2$ where ν is the effective quantum number (although often designated by the principal quantum number n); z is the charge of the ion, and E_c is the excitation energy of the core ion to which the Rydberg series belongs. The intensities and shapes of resonances belonging to a series are also correlated. Our criteria in assigning a Rydberg series consists of relating at least four resonant peaks by energy and by intensity. In addition, the lower peak principal quantum number n should be $n > 3$ (the ground state configuration of Cl III is $3s^23p^3$). In the present measurements, resonant structures are intermingled with strong superposition of various Rydberg series belonging to closely-lying core ion excitation levels. No particular Rydberg series of resonances were identified under the required criteria.

For the purpose of identification of features in the spectrum, we use the theoretical cross sections in Figure 2 as a guide. As mentioned above, Cl III ions were generated (in this experiment) with an ECR ion source. This ion source produces undetermined populations of excited electronic states in the ion beam. Hence, the relative populations of excited states in the ion beam cannot be established, although their presence can be inferred. For instance, the lower panels of Figure 2 show that the zero offset of the relative ion yield of Figure 1 and the structure below 42 eV can be attributed to excited Cl III in the states $(3s3p^4)^4P_{1/2,3/2,5/2}$; $(3s^23p^3)^2P_{1/2,3/2}^\circ$ and $^2D_{3/2,5/2}^\circ$. By matching the positions of the observed resonances and relevant shapes with the calculated ones in Figure 2, we can identify the initial states originating most of the energy resonances in the spectrum, and thus, benchmark the experiment and theory with each other.

The peak at 41.038 eV (labeled as 10 in Figure 1 and in Table 3) is correlated to the Cl III $^2P_{1/2,3/2}^\circ$ initial state. The most prominent resonance in the experimental spectrum at 45.280 eV (labeled as 15 in Figure 1 and in Table 3) can be correlated to the interference of resonant structures from initial Cl III ions in states $^4S^\circ$ (panel b) and $(3s3p^4)^4P$ (panels g to i). Although the intensity does not appear to correspond, it should be noted that the spectrum of Figure 1 is relative. In addition, the indeterminacy of the relative contributions from all possible states could be an explanation for this disagreement. This is, for example, the case for the lower-energy interval of the spectrum where resonance intensities predicted by the theory do not match the experimental spectrum.

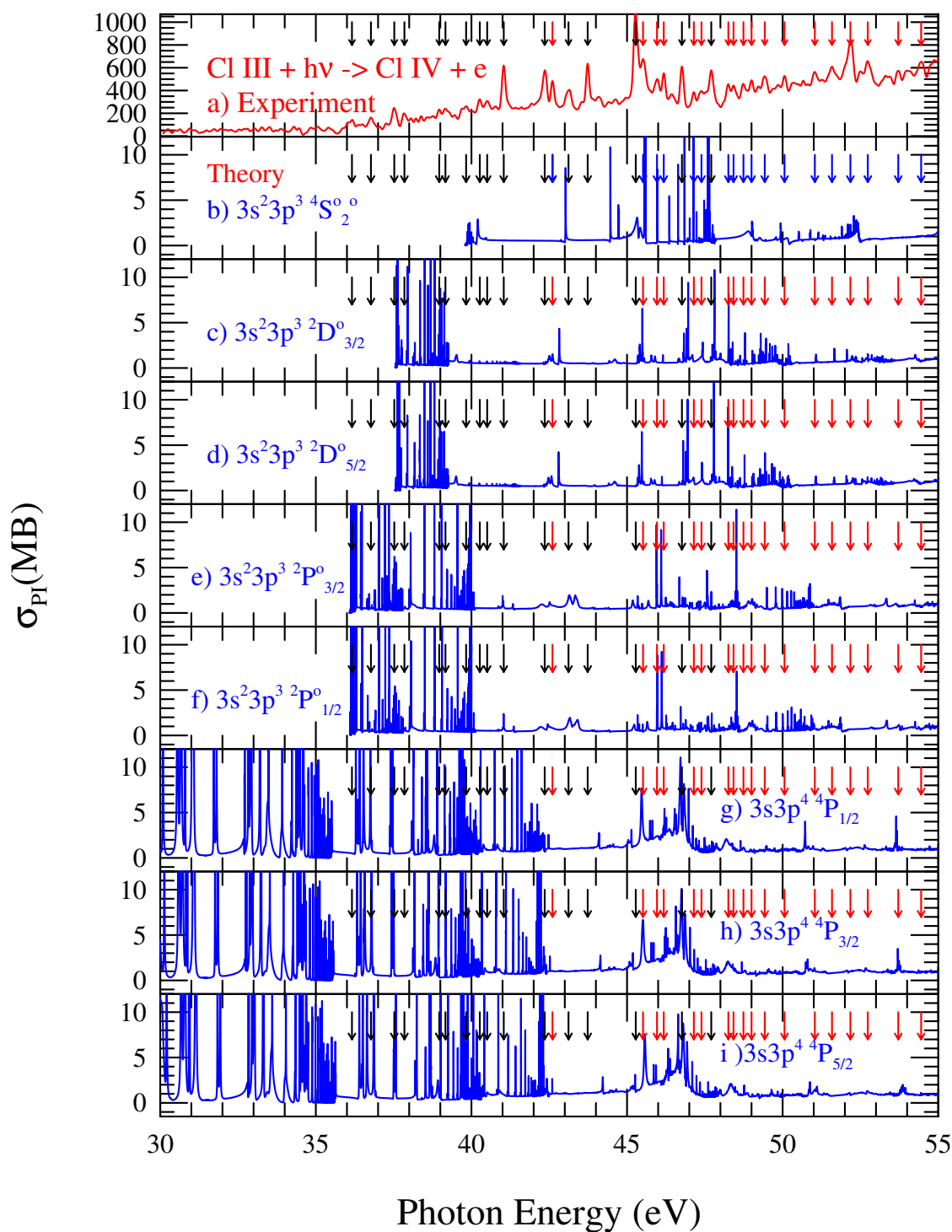


Figure 2. (Color online) Calculated single-photon photoionization ion-yield spectrum of Cl III into Cl IV (blue) in panels (b–i). The top panel (red) corresponds to the measured spectrum of Figure 1. Subsequent panels present the σ_{PI} of the eight lowest levels of Cl III, ground (b) $3s^2 3p^3 (^4S_{3/2}^{\circ})$ and excited (c) $3s^2 3p^3 (^2D_{5/2}^{\circ})$, (d) $3s^2 3p^3 (^2D_{3/2}^{\circ})$, (e) $3s^2 3p^3 (^2P_{3/2}^{\circ})$, (f) $3s^2 3p^3 (^2P_{1/2}^{\circ})$, (g) $3s 3p^4 (^4P_{5/2})$, (h) $3s 3p^4 (^4P_{3/2})$, (i) $3s 3p^4 (^4P_{1/2})$. The first five levels (b–f) show contributions to the observed spectrum by the presence of resonant structures while the three excited levels of $3s 3p^4 (^4P)$ (g–i) show lesser contributions.

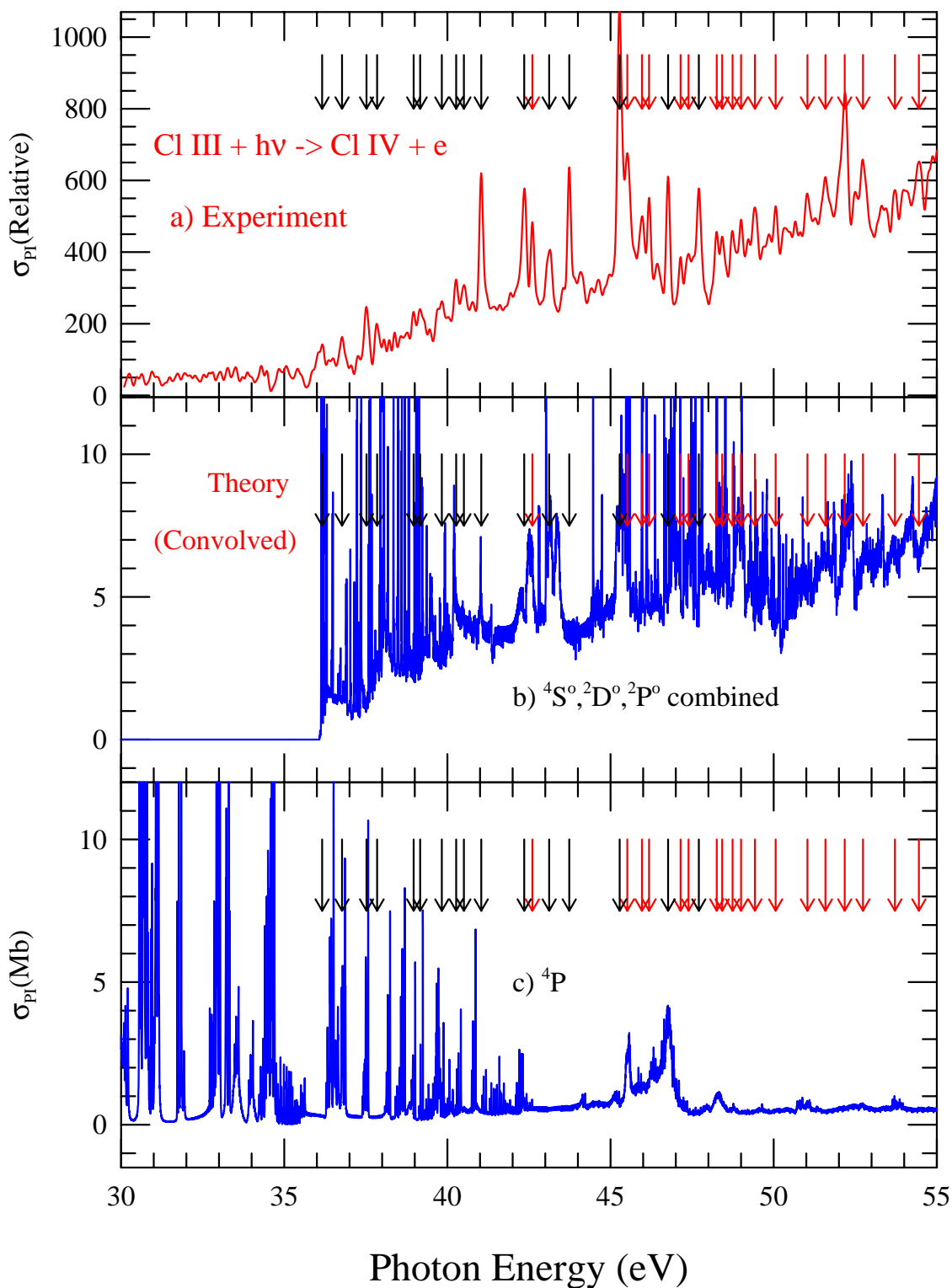


Figure 3. (Color online) Calculated single-photon photoionization (convolved with the Gaussian profile of the experimental beam-width) ion-yield spectrum of Cl III into Cl IV (blue). The top panel corresponds to the measured spectrum of Figure 1 (red). Panel (b) presents the summed features from the convolved σ_{PI} of the lowest five initial levels of states $4S^{\circ}$, $2D^{\circ}$ and $2P^{\circ}$ only. Panel (c) corresponds to the sum σ_{PI} of the three $4P$ initial levels only.

In the present theory, the experimental resolution was simulated by a convolution of the theoretical data with a Gaussian function. Gaussian is an approximate profile. The width of the convolution function was set to 10 meV, but was also reduced in some energy regions to avoid dissolution of some resonances and match the experimental spectrum. These could explain some differences in the resonances intensities. The observed resonance at about 43.8 eV is not found in the predicted spectra of any of the five levels. However, a weak structure can be seen close to the energy in the convolved sum of cross sections for 4P in Figure 3 (the lowest panel). Apart from these considerations, the origin of this particular resonance is unknown.

Often, the predicted resonant lines are suppressed and smeared by the experiment beam width, which is not of a pure Gaussian shape. We note from the comparison of shapes in the observed (panel a) and predicted (panel b) of Figure 3 that the main contributors to the observed spectra came from the five lower-lying levels, $3s^23p^3(^4S_{3/2}^o)$, $3s^23p^3(^2D_{5/2}^o)$, $3s^23p^3(^2D_{3/2}^o)$, $3s^23p^3(^2P_{3/2}^o)$, and a relatively small contribution from the three levels of $3s3p^4(^4P_{1/2,3/2,5/2})$. Good agreement between the observed and the predicted combined spectra in (panel b) of Figure 3 is obtained.

6. Conclusions

A study of the single-photon photoionization of the Cl III ion was carried out with two sophisticated approaches; an experimental approach using the high-resolution ALS synchrotron at LBNL, and a theoretical approach using the powerful R-matrix method. In addition to its fundamental interest, this ion is important because it has been detected in the interstellar medium, and photoionization spectra can therefore provide information on the physical condition and chemical evolution of astrophysical objects. In this experiment, a relative-intensity ion-yield spectrum of Cl IV originating from the photoionization of Cl III was measured with a photon energy resolution of 10 meV. The resulting spectrum was complex, as a monotonically-increasing background signal with several overlapping resonant structures was found. To interpret the spectrum, a relativistic, close-coupling calculation using the Breit–Pauli R-matrix method was implemented. The resulting theoretical spectrum predicts most of the observed resonant structures and the observed increase in the non-resonant background.

Author Contributions: Conceptualization: G.H. and S.N.N.; Methodology: S.N.N. (theory). Software: S.N.N. (R-matrix codes and relevant codes for theoretical analysis). Resources: Ohio Supercomputer Center (computation), Advanced Light Source at Lawrence Berkeley National Laboratory (experiment). Investigation: all authors in the experimental team contributed equally to the experiment execution and analysis and data reduction. All authors have read and agreed to the published version of the manuscript.

Funding: G.H. acknowledges partial funding from UNAM-DGAPA-PAPIIT-IN107420. SNN acknowledges the Ohio Supercomputer Center grant for carrying out all computations. D.H acknowledges financial support from the Swedish Research Council (2016-03650 and 2020-03505).

Data Availability Statement: Photoionization cross section data are available online at NORAD-Atomic-Data website <https://norad.astronomy.osu.edu/>.

Conflicts of Interest: The authors declare no conflict of interest.

References

1. Feldman, P.; Ake, T.; Berman, A.F.; Moos, H. Detection of Chlorine Ions in the Far Ultraviolet Spectroscopic Explorer Spectrum of the Io Plasma Torus. *Astrophys. J.* **2001**, *554*, L123–L126. [[CrossRef](#)]
2. Feldman, P.D. A Spectroscopic Tour of the Solar System with FUSE. In *Astrophysics in the Far Ultraviolet: Five Years of Discovery with FUSE*, *ASP Conf. Series; Proceedings of the Conference, Victoria, BC, Canada 2–6 August 2004*; Sonneborn, G., Moos, H., Andersson, B.-G., Eds.; NASA/Goddard Space Flight Center: Greenbelt, MD, USA, 2006; Volume 348, p. 307.

3. Schneider, N.M.; Park, A.H.; Kupperts, M.E. Spectroscopic Studies of the Io Torus during Galileo Encounters: Remote Plasma Diagnostics and the Detection of Cl^{++} . In Proceedings of the 32nd Meeting of the Division for Planetary Sciences of the American Astronomical Society, Pasadena, CA, USA, 23–27 October 2000; Volume 32, p. 1047.
4. Sylwester, B.; Phillips, K.J.H.; Sylwester, J.; Kuznetsov, V.D. The Solar Flare Chlorine Abundance from RESIK X-ray Spectra. *Astrophys. J.* **2011**, *738*, 49. [[CrossRef](#)]
5. Moomey, D.; Federman, S.R.; Sheffer, Y. Revisiting the Chlorine Abundance in Diffuse Interstellar Clouds from Measurements with the Copernicus Satellite. *Astrophys. J.* **2012**, *744*, 174. [[CrossRef](#)]
6. Hernández, E.; Juárez, A.; Kilcoyne, A.; Aguilar, A.; Hernández, L.; Antillón, A.; Macaluso, D.; Morales-Mori, A.; González-Magaña, O.; Hanstorp, D.; et al. Absolute measurements of chlorine Cl^+ cation single photoionization cross section. *J. Quant. Spectrosc. Radiat. Transf.* **2015**, *151*, 217–223. [[CrossRef](#)]
7. Nahar, S.N. Photoionization features of the ground and excited levels of Cl II and benchmarking with experiment. *New Astron.* **2021**, *82*, 101447. [[CrossRef](#)]
8. Seaton, M.J. Atomic data for opacity calculations. I. General description. *J. Phys. B* **1987**, *20*, 6363. [[CrossRef](#)]
9. Bizau, J.M.; Champeaux, J.P.; Cubaynes, D.; Wuilleumier, F.J.; Folkmann, F.; Jacobsen, T.S.; Penent, F.; Blancard, C.; Kjeldsen, H. Absolute cross sections for L-shell photoionization of the ions N^{2+} , N^{3+} , O^{3+} , O^{4+} , F^{3+} , F^{4+} and Ne^{4+} . *Astron. Astrophys.* **2005**, *439*, 387–399. [[CrossRef](#)]
10. Nahar, S. The IRON Project: Photoionization of Fe ions. *arXiv* **2018**, arXiv:1801.05410.
11. Nahar, S. Database NORAD-Atomic-Data for atomic processes in plasma (Nahar-OSU-Radiative-Atomic-Data). *Atoms* **2020**, *8*, 68. [[CrossRef](#)]
12. Schectman, R.M.; Federman, S.R.; Brown, M.; Cheng, S.; Fritts, M.C.; Irving, R.E.; Gibson, N.D. Oscillator Strengths for Ultraviolet Transitions in Cl II and Cl III. *Astrophys. J.* **2005**, *621*, 1159–1162. [[CrossRef](#)]
13. Tayal, S.S. Strong term dependence of wavefunctions and series perturbations in singly ionized chlorine. *J. Phys. At. Mol. Opt. Phys.* **2003**, *36*, 3239. [[CrossRef](#)]
14. McLaughlin, B.M. Photoionization of Cl^+ from the $3s^2 3p^4 \ ^3P_{2,1,0}$ and the $3s^2 3p^4 \ ^1D_2$, 1S_0 states in the energy range 19–28 eV. *Mon. Not. R. Astron. Soc.* **2016**, *464*, 1990–1999. [[CrossRef](#)]
15. Berkowitz, J.; Greene, J.P.; Cho, H.; Goodman, G.L. Photoionisation of atomic phosphorus. *J. Phys. B At. Mol. Phys.* **1987**, *20*, 2647–2656. [[CrossRef](#)]
16. Westphal, M.S.; Pradhan, A.K. Monte Carlo simulations of biophysical factors for viability of life in exoplanetary atmospheres. In Proceedings of the Workshop on Astrophysical Opacities, Kalamazoo, Michigan, 1–4 August 2017; ASP Conference Series 2018; Volume 515, pp. 249–252.
17. Pradhan, A.K.; Nahar, S.S.N. *Atomic Astrophysics and Spectroscopy*; Cambridge University Press: Cambridge, MA, USA, 2011.
18. Burke, P.; Robb, W. The R-matrix theory of atomic processes. *Adv. At. Mol. Phys.* **1976**, *11*, 143–214.
19. Berrington, K.A.; Burke, P.G.; Butler, K.; Seaton, M.J.; Storey, P.J.; Taylor, K.T.; Yan, Y. Atomic data for opacity calculations. II. Computational methods. *J. Phys. B* **1987**, *20*, 6379. [[CrossRef](#)]
20. Berrington, K.A.; Eissner, W.B.; Norrington, P.H. RMATRIX1: Belfast atomic R-matrix codes. *Comput. Phys. Commun.* **1995**, *92*, 290–420. [[CrossRef](#)]
21. Nahar, S.N.; Pradhan, A.K. Unified treatment of electron-ion recombination in the close-coupling approximation. *Phys. Rev. A* **1994**, *49*, 1816–1835. [[CrossRef](#)] [[PubMed](#)]
22. Zhang, H.L.; Nahar, S.N.; Pradhan, A.K. Close-coupling R-matrix calculations for electron-ion recombination cross sections. *J. Phys. B* **1999**, *32*, 1459. [[CrossRef](#)]
23. Eissner, W.; Jones, M.; Nussbaumer, H. Techniques for the calculation of atomic structures and radiative data including relativistic corrections. *Comput. Phys. Commun.* **1974**, *8*, 270–306. [[CrossRef](#)]
24. Nahar, S.N.; Eissner, W.; Chen, G.X.; Pradhan, A.K. Atomic data from the Iron Project: LIII. Relativistic allowed and forbidden transition probabilities for Fe XVII. *Astron. Astrophys.* **2003**, *408*, 789–801. [[CrossRef](#)]
25. Martin, W.C.; Kaufman, V.; Sugar, J.; Musgrove, A. Preliminary Compilation of Wavelengths and Energy-Levels for the Spectra of Chlorine (Unpublished), 1992–1997. Available online: <https://physics.nist.gov/asd> (accessed on 1 July 2020).
26. Kramida, A.; Ralchenko, Y.; Reader, J.; NIST ASD Team. *NIST Atomic Spectra Database (ver. 5.9)*; National Institute of Standards and Technology: Gaithersburg, MD, USA, 2021. Available online: <http://physics.nist.gov/asd> (accessed on 1 July 2020). [[CrossRef](#)]
27. Nahar, S. Photoionization cross sections of O II, O III, O IV, and O V: Benchmarking R-matrix theory and experiments. *Phys. Rev. A* **2004**, *69*, 042714. [[CrossRef](#)]
28. Phaneuf, R.A.; Havener, C.C.; Dunn, G.H.; Muller, A. Merged-beams experiments in atomic and molecular physics. *Rep. Prog. Phys.* **1999**, *62*, 1143. [[CrossRef](#)]
29. Covington, A.M.; Aguilar, A.C.; Covington, I.R.; Gharaibeh, M.F.; Hinojosa, G.; Shirley, C.A.; Phaneuf, R.A.; Álvarez, I.; Cisneros, C.; Dominguez-Lopez, I.; et al. Photoionization of Ne^+ using synchrotron radiation. *Phys. Rev. A* **2002**, *66*, 062710. [[CrossRef](#)]
30. Esteves, D.A.; Bilodeau, R.C.; Sterling, N.C.; Phaneuf, R.A.; Kilcoyne, A.L.D.; Red, E.C.; Aguilar, A. Absolute high-resolution Se^+ photoionization cross-section measurements with Rydberg-series analysis. *Phys. Rev. A* **2011**, *84*, 013406. [[CrossRef](#)]
31. Müller, A.; Schippers, S.; Hellhund, J.; Holste, K.; Kilcoyne, A.L.D.; Phaneuf, R.A.; Ballance, C.P.; McLaughlin, B.M. Single-photon single ionization of W^+ ions: Experiment and theory. *J. Phys. B At. Mol. Opt. Phys.* **2015**, *48*, 235203. [[CrossRef](#)]

32. Domke, M.; Schulz, K.; Remmers, G.; Kaindl, G.; Wintgen, D. High-resolution study of $1P^0$ double-excitation states in helium. *Phys. Rev. A* **1996**, *53*, 1424–1438. [[CrossRef](#)]
33. King, G.C.; Tronc, M.; Read, F.H.; Bradford, R.C. An investigation of the structure near the $L_{2,3}$ edges of argon, the $M_{4,5}$ edges of krypton and the $N_{4,5}$ edges of xenon, using electron impact with high resolution. *J. Phys. B* **1977**, *10*, 2479–2495. [[CrossRef](#)]

Disclaimer/Publisher’s Note: The statements, opinions and data contained in all publications are solely those of the individual author(s) and contributor(s) and not of MDPI and/or the editor(s). MDPI and/or the editor(s) disclaim responsibility for any injury to people or property resulting from any ideas, methods, instructions or products referred to in the content.